Journal of the European Ceramic Society 39 (2019) 2846–2854

Contents lists available at ScienceDirect

Journal of the European Ceramic Society

journal homepage: www.elsevier.com/locate/jeurceramsoc

Original Article

Carbon content and pyrolysis atmosphere effects on phase development in SiOC systems

Kaustubh Bawane, Donald Erb, Kathy Lu*

Department of Materials Science and Engineering, Virginia Polytechnic Institute and State University, Blacksburg, VA, 24061, USA

ARTICLE INFO

Keywords:
Silicon oxycarbide
Carbon content
Pyrolysis atmosphere
Phase percent
Microstructure
Thermodynamic analysis

ABSTRACT

In this study, bulk silicon oxycarbides (SiOCs) were fabricated from base polysiloxane (PSO) systems with different carbon content by using Ar or Ar + H_2O pyrolysis atmosphere. Compared to the Ar pyrolysis condition, the SiOC samples pyrolyzed with water vapor plus Ar generally show lower ceramic yield except for the Tospearl (polymethylsilsesquioxane) sample at 1400 °C. The SiOC ceramics contain significantly less SiC and carbon after pyrolysis under Ar + H_2O atmosphere compared to pure Ar atmosphere. The carbon-poor Tospearl sample shows a crystalline SiO_2 structure (cristobalite) after pyrolysis at 1400 °C in Ar + H_2O, which is also confirmed using TEM diffraction pattern analysis. TEM microstructures indicate little change in microstructures for the carbon-rich samples. The fundamentals, such as total Gibbs free energy, the driving force for crystallization, and phase contents at different pyrolysis temperatures can be calculated based on a Gibbs free energy minimization method. The phase content calculations predict considerable decrease in the amounts of SiC and C and significant increase in the percent of SiO_2 after pyrolysis in Ar + H_2O compared to Ar. The thermodynamic calculation results match with our experimental observations. This work provides a guided method to synthesize high temperature SiOCs with desired phases.

1. Introduction

Silicon oxycarbides (SiOCs) are novel polymer derived ceramics that show high flexibility in tailoring microstructures and phases with a composition of SiC_xO_{4-x} ($1 \le x \le 3$) [1]. At lower pyrolysis temperatures (800–1000 °C), SiOC consists of a homogeneous network of mixed Si−C−O tetrahedral and polyaromatic carbon species. It has an amorphous structure, in which Si atoms share chemical bonds with O and C atoms. At higher temperatures (> 1100 °C), SiOC decomposes into more thermodynamically stable species (e.g., β-SiC), amorphous SiO_2-rich nanodomains (mainly SiO_2 although some Si−O−C species are still present), and highly disordered graphite-like carbon (termed as free carbon) [2,3]. Depending on the microstructure, the properties of the SiOCs, such as electrical conductivity and oxidation resistance, can be greatly altered [4–6].

SiOC can be expressed as $SiO_{2(1-x)}C_x + yC_{free}$, where x + y is the molar ratio of the C content relative to the Si content [7]. Different C contents influence the compositions, structural characteristics, and phase changes of SiOCs. Compositions of SiOCs play important roles in their properties, especially the thermal behaviors, electric conductivity, and mechanical properties of the resulting materials.

Many studies attempt to adjust the compositions of SiOCs through the selection of precursors, mainly by adjusting the resulting content of free carbon [8,9]. Narisawa et al. [10] reported SiOC ceramics with long-lived photoluminescence by pyrolysis of Tospearl 120 (chemical composition of $SiO_{1.66}C_{1.00}H_{3.36}$) in a reducing atmosphere of H_2. Blum et al. [11] investigated porous SiOC ceramics by pyrolysis of polyhydromethylsiloxane (PHMS) and vinyl-terminated polydimethylsiloxane (PDMS) of different molecular weights as precursor materials. Various methods were reported for tailoring the chemical compositions of SiOCs that contain a high C content. For example, Hourlier et al. [12] used aromatic crosslinker divinylbenzene (DVB) and introduced a significantly higher C content compared to tetramethyl-tetravinyl cyclotetrasiloxane (TMTVS). Crosslinking agents containing Si−CH=CH_2 were also used to initiate the hydrosilylation reaction [13] and increase the C content, though to a lesser extent.

The second method to control the phases formed during pyrolysis is by introducing reactive species into the pyrolysis atmosphere, such as H_2, H_2O, or CO_2 [1,14–17]. Several studies have shown that water vapor injection during the temperature range at which the chemical bonds in the polymer break results in an increase in Si−O−Si bonds and decrease in Si−C bonds [1,15,16]. Narisawa et al. [17] investigated the dependence of SiOC chemical compositions and molecular structures on their reaction conditions by varying the pyrolysis atmospheres (H_2, Ar,

* Corresponding author.
E-mail address: klu@vt.edu (K. Lu).

https://doi.org/10.1016/j.jeurceramsoc.2019.03.032
Received 20 January 2019; Received in revised form 9 March 2019; Accepted 13 March 2019
Available online 15 March 2019
0955-2219/

and CO_2). The chemical composition, color, residual mass, and electron spin resonance of the SiOC ceramics differ depending on the pyrolysis atmosphere. Compared to the sample pyrolyzed in Ar, the H_2 pyrolyzed sample contains no free carbon within the SiOC, and the CO_2 pyrolyzed sample contains no Si—C bonds [17].

In this study, we selected polysiloxanes with different carbon content as precursors, and then synthesized different amorphous SiOC ceramics by using Ar or Ar + H_2O atmosphere during pyrolysis. The derived SiOC ceramics were characterized using X-ray diffraction (XRD) and transmission electron microscopy (TEM). Carbon content and pyrolysis atmosphere effects on the phase development of the SiOCs were studied. The differences in phase formation due to both carbon content and pyrolysis atmosphere were investigated using thermodynamic modelling to compute the driving force for crystallization as well as phase fractions in the various systems.

2. Experimental procedures

The chemicals were obtained from Gelest Inc., Morrisville, PA. All chemicals were of analytical grade and were used without further purification. To investigate the effects of different C-containing side groups from precursors, polyhydromethylsiloxane (PHMS), vinyl terminated polydimethylsiloxane (PDMS), polyvinylmethylsiloxane (PVMS), and vinyl terminated polyphenylmethylsiloxane (PMPS) were used as starting materials. For lower C content samples, the precursor used was Tospearl 120 (polymethylsilsesquioxane, Momentive Performance Materials, Tokyo, Japan), which was made up of densely crosslinked silicone resin particles with an average diameter of 2 μm. 2.1–2.4 wt% platinum-divinyltetramethyldisiloxane complex in xylene (Pt catalyst) was used as the catalyst.

PDMS, PVMS, and PMPS samples were obtained by catalytic crosslinking of PDMS (or PVMS, or PMPS) and PHMS. The PHMS/PDMS (PVMS or PMPS) weight ratio was 15/85. First, solutions with the polymer precursor (PDMS or PVMS or PMPS) and PHMS were sonicated for 10 min and then mixed in a high energy mill (SPEX 8000 M Mixer/Mill, SPEX Sample Prep, Metuchen, NJ) for 10 min to form a homogeneous mixture. Next, the Pt catalyst (5 ppm Pt relative to PHMS) was added, the mixtures were mixed again in the high energy ball mill for 5 min, and then poured into aluminum foil molds. The mixtures were placed into a vacuum chamber and vacuumed for 10 min at 1500 mTorr to remove any bubbles in the solutions. The filled molds were then placed in an oven to crosslink at 50 °C for 12 h and then at 120 °C for 6 h. When crosslinking PHMS, only 2.5 ppm of the above Pt catalyst solution was added in order to slow down the crosslinking and avoid defect formation; other steps were the same. To prepare the samples for pyrolysis, the cured materials were first cut and polished to roughly 13 mm × 13 mm × 3 mm size. The as-received Tospearl powder was pressed into circular pieces with a diameter of 13 mm and a thickness of 3 mm using 10 wt% PHMS as a binder at a pressure of ~500 MPa.

Next, the samples were placed into a zirconia crucible between two graphite melts to reduce friction forces due to the shrinkage of the green bodies during pyrolysis and allow for uniform outgassing of volatiles during ceramization. They were then put into a tube furnace (1730-20 Horizontal Tube Furnace, CM Furnaces Inc., Bloomfield, NJ). The samples were pyrolyzed in an Ar atmosphere with a flow rate of about 900 std cm^3/min at 1300 °C and 1400 °C, respectively, with a heating rate of 1 °C/min for 2 h, then cooled to 400 °C with a rate of 1 °C/min, and finally cooled to 50 °C with a rate of 2 °C/min.

To compare the effect of water injection on the properties of the SiOC samples, similar experiments were carried out by pyrolysis of the green bodies with water injection using the same pyrolysis conditions. The temperature range of water injection was chosen at 500 °C–700 °C for 2 h, as the polymer to ceramic transformation and carbon precipitation mainly occur in this temperature range [18]. The argon flow rate was ~500 cm^3 std/min. The Ar:H_2O molar ratio was ~5:1. The temperature was then raised to 1300 °C and 1400 °C with a holding time of 120 min, and then cooled down as for the Ar atmosphere. At 1300 °C or 1400 °C pyrolysis temperature, SiOCs with different amounts of C were synthesized in an Ar + H_2O atmosphere.

The phase compositions of the pyrolyzed samples were analyzed in an X'Pert PRO diffractometer (PANalytical B.V., EA Almelo, the Netherlands) with Cu Kα radiation. The microstructures of the pyrolyzed ceramics were studied using a transmission electron microscope (JEOL 2100, JEOL USA, Peabody, MA); the samples were prepared by grinding the bulk specimens in a mortar and then dispersing them in absolute ethanol. The compositions of the samples were analyzed by a combustion method for carbon and an ICP-OES method for silicon. Acid digestion and titration were used to obtain the silicon content. The oxygen content was extracted based on the above results and the total mass of the samples. These experiments were conducted by Galbraith Laboratories, Inc. (Knoxville, TN) based on multiple measurements.

Thermodynamic simulations were carried out by developing a Gibbs free energy minimization program on the Mathematica software. Phase fractions and driving energy for crystallization were calculated for various SiOC compositions.

3. Results and discussion

3.1. Phase evolution

Fig. 1(a) shows the XRD patterns for the SiOC samples pyrolyzed from Tospearl, PDMS, and PMPS in Ar or Ar + H_2O at 1300 °C. The XRD patterns for the SiOCs pyrolyzed from the PHMS and PVMS precursors are shown in the supplement, Fig. S1. In Ar, the PHMS, PDMS,

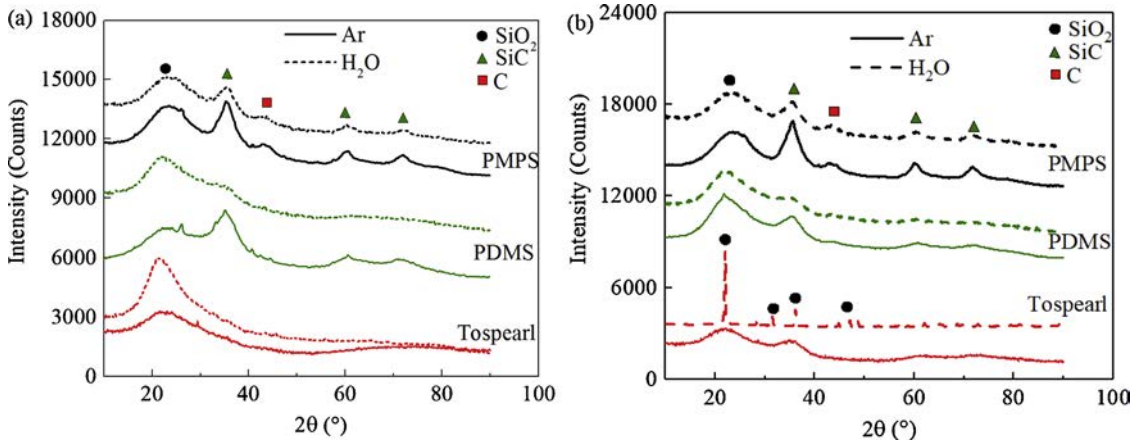

Fig. 1. XRD patterns for the Tospearl, PDMS, and PMPS samples pyrolyzed at (a) 1300 °C and (b) 1400 °C.

Table 1
Ceramic yield of the SiOC samples after 1300 and 1400 °C pyrolysis.

Pyrolysis temperature	Sample	Pyrolysis atmosphere	
		Ar	Ar + H_2O
1300 °C	Tospearl	80.2 ± 0.1	78.6 ± 0.6
	PHMS	84.6 ± 0.3	53.6 ± 2.0
	PDMS	75.0 ± 1.2	22.2 ± 3.3
	PVMS	78.7 ± 0. 5	71.9 ± 3.5
	PMPS	78.6 ± 1.1	50.1 ± 3.1
1400 °C	Tospearl	67.7 ± 0.7	78.9 ± 0.1
	PHMS	83.4 ± 0.7	53.5 ± 15.7
	PDMS	74.6 ± 2.46	29.6 ± 9.1
	PVMS	78.5 ± 2.16	76.0 ± 3.2
	PMPS	74.5 ± 1.7	57.2 ± 7.8

PVMS, and PMPS samples exhibit a very broad peak at ~22°, which is attributed to amorphous SiO_2, and the shoulder peaks centering at 26.2°and 44.4° are indexed to be graphite (JCPDS Card No. 00-075-1621). The diffraction peaks at 35.7°, 60.1°, and 71.9° correspond to the (111), (220), and (311) crystalline planes of the β-SiC phase (JCPDS Card No. 01-073-1665). The SiO_2, SiC, and graphite diffraction peaks appear due to the phase separation of SiOC, as well as the carbothermal reduction of SiO_2 into SiC by Eqs. (1) and (2).

$$2SiOC \rightarrow SiO_2\ (amorphous) + C\ (graphite) + SiC\ (\beta) \quad (1)$$

$$SiO_2\ (amorphous) + 3C\ (graphite) \rightarrow SiC\ (\beta) + 2CO\ (g) \quad (2)$$

Eq. (1) represents the SiOC phase separation into amorphous SiO_2, SiC(β), and graphitic carbon at low pyrolysis temperatures (800–1100 °C) [19]. Eq. (2) indicates that carbothermal reaction occurs between SiO_2 and graphite, producing SiC(β) and CO gas at above 1100 °C [2]. When introducing more C into the sample (PVMS or PMPS), the vinyl or phenyl groups lead to more volatile species and pyrolyze into more free C at high temperatures. This explains why the C peaks are observed.

In Ar + H_2O, the PHMS, PDMS, PVMS, and PMPS samples show reduced SiC peaks at 35.7°, 60.1°, and 71.9° compared to the samples pyrolyzed in Ar due to the decrease of free C and thus Si—C bonds in the water vapor environment. With the presence of water vapor between 500-700 °C, the polymer to ceramic transformation occurs with the following additional possible reactions [14,15]:

$$Si-H\ (s) + H_2O(g) \rightarrow Si-OH\ (s) + H_2\ (g) \quad (3)$$

$$Si-CH_3\ (s) + H_2O\ (g) \rightarrow Si-OH\ (s) + CH_4\ (g) \quad (4)$$

$$Si-CH=CH_2\ (s) + H_2O\ (g) \rightarrow Si-OH\ (s) + C_2H_4\ (g) \quad (5)$$

$$Si-C_6H_5\ (g) + H_2O\ (g) \rightarrow Si-OH\ (s) + C_6H_6\ (g) \quad (6)$$

The Si—OH bonds further condense to form Si—O—Si bonds:

$$Si-OH\ (s) + Si-OH\ (s) \rightarrow Si-O-Si\ (s) + H_2O\ (g) \quad (7)$$

In addition, the free C that precipitates between 500-700 °C also oxidizes following the reaction [1,14,20]:

$$C\ (free) + H_2O\ (g) \rightarrow H_2\ (g) + CO\ (g) \quad (8)$$

According to Eqs. (3)–(8), water vapor facilitates Si—O bond formation while reducing Si—C bonds and consuming free carbon; the X-ray diffraction patterns in Fig. 1(a) for all of the samples clearly reflect this. The Tospearl sample shows an amorphous structure with only the presence of the SiO_2 halo centered at ~22°, which means that the phase separation is not present at 1300 °C due to the relatively carbon-poor nature.

Fig. 1(b) shows the XRD patterns for the Tospearl, PDMS, and PMPS samples pyrolyzed in Ar or Ar + H_2O at 1400 °C. The XRD patterns for the SiOCs pyrolyzed from the PHMS and PVMS precursors are shown in the supplement, Fig. S2. In Ar, the PHMS, PDMS, PVMS, and PMPS samples show strong SiC peaks at 35.7°, 60.1°, and 71.9° compared to the samples pyrolyzed at 1300 °C. With further pyrolysis temperature increase, the β-SiC peaks become more intense, indicating an enhancement of β-SiC crystallization. This is because the temperature increase, another important parameter influencing SiC crystallization, promotes the carbothermal reaction and generates more SiC(β) [21–23]. In the same way as at 1300 °C, in Ar + H_2O, the PHMS, PDMS, PVMS, and PMPS samples show reduced SiC peaks compared to the samples pyrolyzed in Ar due to the decrease of Si—C bonds in the water vapor environment.

The XRD patterns of the Tospearl sample pyrolyzed at 1400 °C in Ar shows an amorphous structure with only the presence of the SiO_2 halo centered at ~22° and the SiC peak at 35.7° [24], which means that the phase separation is about to happen. In Ar + H_2O, the diffraction peaks at 22.0°, 28.4°, 31.4°, 46.9, and 48.5° correspond to the (101), (111), (102), (113), and (212) crystalline planes of the cristobalite SiO_2 phase (JCPDS Card No. 01-071-0785). The SiO_2 crystallization is activated due to the C loss as well as the conversion of Si—C bonds into Si—O bonds (Eqs. (7) and (8)). In addition, there is not enough carbon to form SiC. Thus, SiO_2 crystals are produced at 1400 °C pyrolysis (Eq. (9)).

$$2SiOC\ (s) \rightarrow SiO_2\ (crystal) + C\ (graphite) + SiC\ (\beta) \quad (9)$$

During the Ar + H_2O atmosphere pyrolysis, SiO_2 nanodomains form due to phase separation, and the Si—O—Si bonds crystallize into SiO_2 nanocrystals (Eq. (9)) [19].

3.2. Ceramic yield

Table 1 shows the ceramic yield for the SiOC samples. As the pyrolysis temperature increases in Ar, the yield generally decreases, from 80.2% at 1300 °C to 67.7% at 1400 °C for the Tospearl sample, and from 78.6% at 1300 °C to 74.5% at 1400 °C for the PMPS sample (the PHMS, PDMS, and PVMS samples have the same trend). The changes of the ceramic yield are related to the pyrolysis process. Eqs. (1) and (2) indicate that carbothermal reaction occurs between SiO_2 and graphite, producing SiC(β) and CO gas, leading to the ceramic yield decreases. Therefore, for the same precursor compositions, increasing pyrolysis temperature leads to more SiC formation and CO release, thus lower ceramic yield.

When introducing more C into the sample (PVMS or PMPS), the vinyl or phenyl groups lead to more volatile species and pyrolyze into more free C at high temperatures. Higher C formation in general leads to lower ceramic yield. However, due to the difference in drastic bond-breaking and re-organization, the trend is not predictable for the carbon-rich precursors as shown in Table 1.

Compared to the Ar pyrolysis, the SiOC samples pyrolyzed with water vapor injection generally show lower ceramic yield except for the Tospearl sample at 1400 °C. The decrease in the ceramic yield for the Ar + H_2O samples is because water vapor pyrolysis can significantly remove carbon from the resulting SiOCs and produce small evaporative gas molecules, according to Eqs. (3)–(8) [15]. Moreover, the yields of the PHMS, PDMS, and PMPS samples are much lower, because losses of small gas molecules are more likely to occur. This is especially the case for PDMS. However, it is difficult to predict the trend based on the precursors. The most likely reason is that the more C-rich nature of the precursors leads to more C loss under the H_2O atmosphere while the precursors themselves are not able to hydrolyze (such as for PHMS). However, since the precursors undergo bond breaking and bond rearrangement continuously during pyrolysis, the exact reactions with water vapor for each of the precursors need to be further studied. For the Tospearl sample, the ceramic yield increases from 67.7% in Ar to 78.9% in Ar + H_2O, which can be attributed to the SiO_2 enrichment due to the conversion of Si—C bonds to Si—O bonds, as discussed previously. Further, the slight increase in the ceramic yield for the Ar + H_2O samples with increasing pyrolysis temperature is simply due to experimental uncertainty.

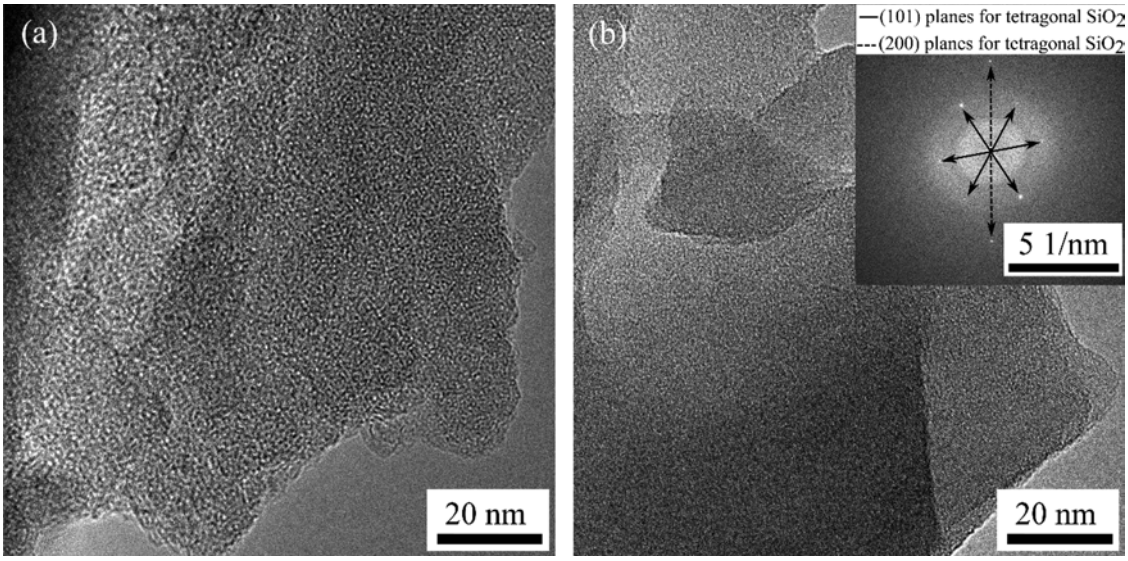

Fig. 2. TEM images for the Tospearl pyrolyzed at 1400 °C in (a) Ar and (b) Ar + H_2O. The inset of (b) is the FFT of the entire image.

3.3. Microstructure

The microstructures of the Tospearl samples pyrolyzed at 1400 °C in Ar or Ar + H_2O are shown in Fig. 2. For the sample pyrolyzed in Ar, the sample is mostly amorphous due to the dominance of the SiOC phase. Because of the low carbon content of the polymer precursor, the pyrolyzed ceramic does not contain a significant concentration of free carbon. Although nanocrystalline SiC is detectable using XRD, the crystallites must be of such a fine size and low concentration that they are not distinguishable from the amorphous SiOC under TEM. For the Tospearl sample pyrolyzed in Ar + H_2O, although the examined region does not show any specific features, a fast Fourier transform (FFT) of Fig. 2(b) is displayed in the inset, showing diffraction spots corresponding to a crystalline polymorph of cristobalite SiO_2.

The PMPS sample pyrolyzed in Ar at 1400 °C (Fig. 3(a)) contains a significant amount of tortuous free carbon (red, wiggly lines) and SiC crystallites (yellow circles), similar to other carbon-rich SiOCs [25,26]. With the water vapor treatment (Fig. 3(b)), the PMPS microstructure is not changed significantly, still containing both graphitic carbon (red, wiggly lines) and SiC crystallites (yellow circles), in agreement with the XRD results (Fig. 1(b)).

3.4. Thermodynamic analysis

Fig. 4 shows the schematic composition diagram for a given SiOC system. SiO_aC_b represents the overall composition of a given sample. The phase separation mechanism of a SiOC system can be divided into two steps. First, the system phase separates into free carbon and amorphous SiO_xC_y located on the tie-line between the SiO_2 and SiC phases as shown in Fig. 4(a). The second step involves phase separation of the SiO_xC_y phase into SiC, SiO_2, and other intermediate SiOC compounds ($SiO_{(4-i)/2}C_{i/4}$ (where i = 1 to 3)) located along the SiC-SiO_2 tie-line as shown in Fig. 4(a).

The phase separation of SiO_aC_b into free carbon and SiO_xC_y can be visualized using the C-SiO_xC_y tie-line in Fig. 4(a). The reaction is given in Eq. (10), where f_c is the fraction of the free carbon phase.

$$SiO_aC_b = f_c \cdot C + (1 - f_c) \cdot SiO_xC_y \quad (10)$$

It can be observed from Fig. 4 that the Si and O compositions along the C-SiO_xC_y tie-line remain the same. Therefore, value 'x' should be the

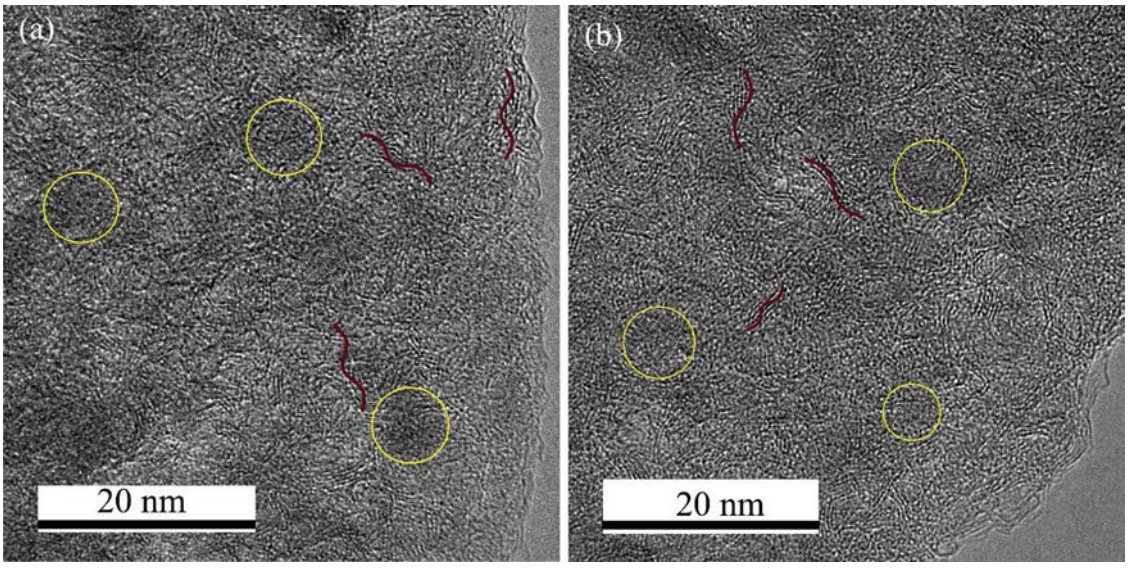

Fig. 3. TEM images for the PMPS pyrolyzed at 1400 °C in (a) Ar and (b) Ar + H_2O.

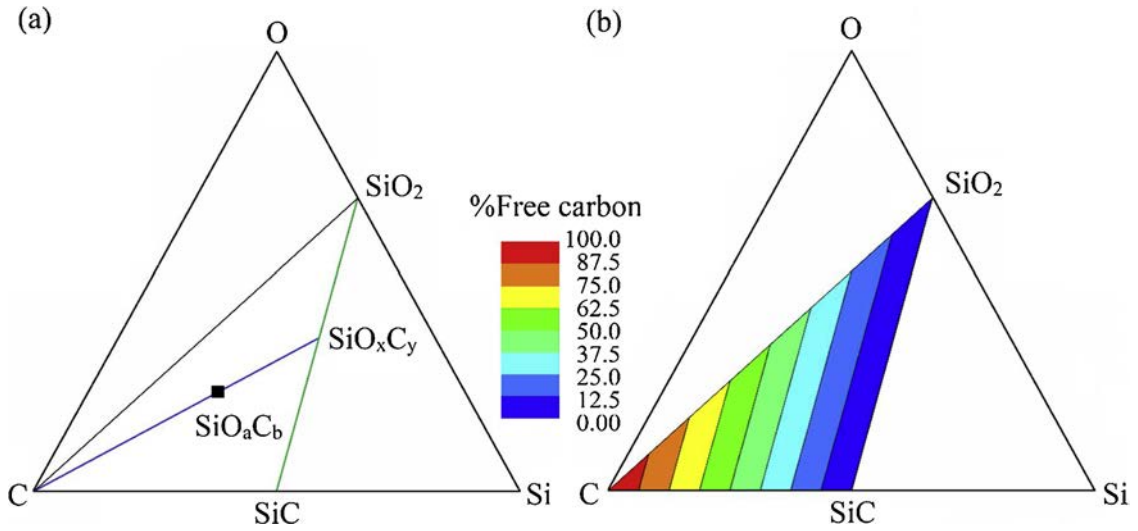

Fig. 4. (a) Schematic composition diagram of a SiOC system, (b) 2D contour plot of different free carbon phase percent in the SiOC composition diagram.

same as 'a'. Since SiO_xC_y can also be represented as $SiO_{(4-i)/2}C_{i/4}$ (where i = 0 to 4) to account for the stoichiometric requirement of the SiO_2-SiC tie-line, the following equation can be derived:

$$y = \frac{4-2x}{4} = \frac{4-2a}{4} \tag{11}$$

It is clear from the composition diagram in Fig. 4 that SiO_aC_b is rich in carbon compared to SiO_xC_y. Therefore, the amount of free carbon and the fraction of free carbon (f_c) can be represented based on Eqs. (13) and (14) respectively. Fig. 4(b) shows the 2D contour plot of free carbon phase percent calculated using Eq. (14). Fig. 4(b) also depicts the compositions of different SiOC systems from this work. The respective free carbon content for each SiOC system can be estimated using the 2D contour plot in Fig. 4(b).

$$\textit{Amount of free carbon} = b - y = b - \frac{4-2a}{4} \tag{12}$$

$$f_c = \frac{b-y}{1+a+b} = \frac{b-\frac{4-2a}{4}}{1+a+b} \tag{13}$$

In the second step, the remaining SiO_xC_y phase separates along the SiO_2-SiC tie-line. As discussed earlier, the compositions along the SiO_2-SiC tie-line can also be represented as $SiO_{(4-i)/2}C_{i/4}$, where i = 0 to 4. Eq. (14) shows the phase separation reaction of SiO_xC_y, where f_0, f_1, f_2, f_3 and f_4 represent the fractions of the corresponding phases.

$$= f_o\cdot(SiO_2) + f_1\cdot\left(SiO_{\frac{3}{2}}C_{\frac{1}{4}}\right) + f_2\cdot\left(SiOC_{\frac{1}{2}}\right) + f_3\cdot\left(SiO_{\frac{1}{2}}C_{\frac{3}{4}}\right) + f_4\cdot(SiC) \tag{14}$$

The overall Gibbs free energy of the phase separated amorphous SiO_xC_y system can be represented using the conventional formula:

$$G^{am-SiOC} = \sum_0^4 f_i(T)\cdot G_i(T) + RT\sum_0^4 f_i(T)\cdot\log f_i(T) \tag{15}$$

The stable configuration of a given SiO_xC_y system depends on the minimum total Gibbs free energy ($G^{am\text{-}SiOC}$). Therefore, the fractions of various phases (f_i) can be calculated for a particular temperature by minimizing $G^{am\text{-}SiOC}$ (Eq. (15)), obeying the stoichiometric constraints shown in Eq. (14). In this paper, the Mathematica software has been used to solve this minimization problem and the codes with an example system are given in the supplement.

The thermodynamic evolution of the SiOC ceramics with different carbon contents can be evaluated following a similar procedure as used for SiCN ceramics [27]. First, it is important to establish values of Gibbs free energy for all the phases ($G_i(T)$, see Eq. (15)). The Gibbs free energy of the crystalline phases are obtained using available data for SiC [27] and cristobalite [28]. Then the Gibbs free energy for the amorphous counterparts are calculated by:

$$G^{amorphous}(T) = G^{crystalline}(T) + \Delta E \tag{16}$$

where ΔE is the vitrification enthalpy. ΔE for SiC, SiO_2, and C are 54 kJ/mol [29], 6.9 kJ/mol [30], and 20.8 kJ/mol [31], respectively. Thus, $G^{am-SiO_2}(T)$ or $G_0(T) = G^{cr-SiO_2} + 6.9$ kJ/mol and $G^{am-SiC}(T)$ or $G_4(T) = G^{cr-SiC}(T) + 54$ kJ/mol. The Gibbs free energies of intermediate compositions, i.e., G_1 (for $SiO_{\frac{3}{2}}C_{\frac{1}{4}}$), G_2 (for $SiOC_{\frac{1}{2}}$), and G_3 (for $SiO_{\frac{1}{2}}C_{\frac{3}{4}}$) can be calculated by assuming their structure as mixed tetrahedra with $SiO_{(4-i)}C_i$ (where i = 1 to 3) compositions. By following a similar mathematical treatment [27], the equation for $G_i(T)$ is given as:

$$G_i(T) = i\,E_{Si-C} + (4-i)E_{Si-O} \tag{17}$$

$$E_{Si\text{-}C} = \frac{1}{4}G^{cr-SiC}(T_0) \tag{18}$$

$$E_{Si\text{-}O} = \frac{1}{4}G^{cr-SiO_2}(T_0) \tag{19}$$

where T_0 is the temperature at which the mixed $SiO_{4-i}C_i$ units form. Taking T_0 to be 1100 K, then $G_1 = -805.8$ kJ/mol, $G_2 = -583.1$ kJ/mol, and $G_3 = -360.5$ kJ/mol. Fig. 5 shows Gibbs free energies for

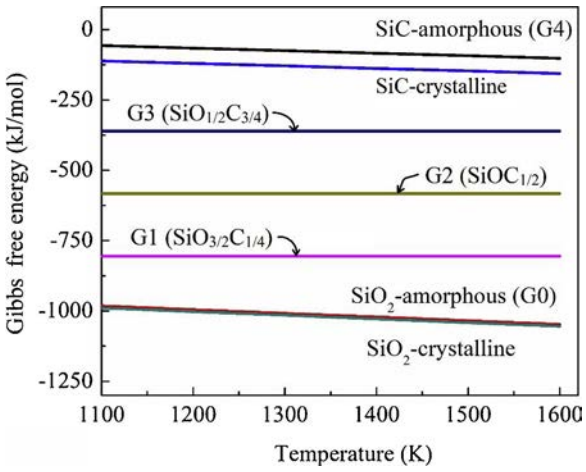

Fig. 5. Gibbs free energies of amorphous and crystalline phases in the SiOC system.

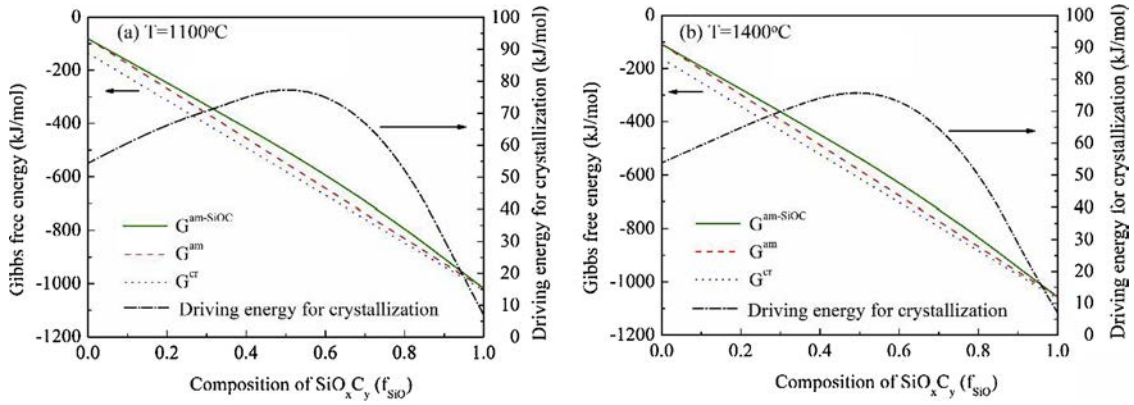

Fig. 6. Minimized Gibbs free energy and driving force for crystallization of the amorphous SiOC system vs. the SiO_xC_y composition: (a) 1100 °C, (b) 1400 °C.

amorphous and crystalline SiC and SiO_2 phases as well as amorphous intermediate phases plotted against pyrolysis temperature. Such Gibbs free energy data are used in the Gibbs free energy minimization program to calculate the fractions of the phases involved.

The composition of SiO_xC_y along the SiC-SiO_2 tie-line (Fig. 4(a)) can also be expressed in terms of the effective fraction of the SiO_2 phase, f_{SiO} (no phase separation into intermediate compositions), which can be calculated using the lever rule:

$$f_{SiO} = \frac{\text{compositon of O in } SiO_xC_y - \text{compositon of O in SiC}}{\text{composition of O in } SiO_2 - \text{compositon of O in SiC}} = \frac{\frac{x}{1+x+y} - 0}{\frac{2}{3} - 0} = \frac{3x}{2(1+x+y)} \quad (20)$$

The Gibbs free energies, assuming no phase separation of SiO_xC_y into intermediate SiOC compounds (i.e., only terminal SiO_2 and SiC), can be calculated as follows:

$$G^{am} = f_{SiO}.\ G^{am-SiO2} + (1 - f_{SiO}).\ G^{am-SiC} \quad (21)$$

$$G^{cr} = f_{SiO}.\ G^{cr-SiO2} + (1 - f_{SiO}).\ G^{cr-SiC} \quad (22)$$

Fig. 6 shows minimized Gibbs free energy ($G^{am\text{-}SiOC}$) calculated by the Mathematica Gibbs free energy minimization program as well as the reference Gibbs free energies (G^{am} and G^{cr}) per Eq. (14) for various SiO_xC_y compositions (f_{SiO}) at 1100 °C and 1400 °C. The driving force for crystallization calculated using Eq. (23) is also plotted on the secondary y-axis in Fig. 6.

$$Driving\ \ force\ \ for\ crystallization = G^{am-SiOC} - G^{cr} \quad (23)$$

Fig. 6 shows that the highest driving force for crystallization is at $f_{SiO} = 0.55$. This means that the SiOC system with this composition will show the least resistance to crystallization during pyrolysis. Fig. 7 shows fractions of the involving phases at different SiO_xC_y compositions calculated by the Mathematica program after 1100 °C and 1400 °C pyrolysis. Therefore, by using the 2D contours in Fig. 4(b) for free carbon percent, and the phase fractions in Fig. 7, the phase separation behavior of any SiOC system can be estimated.

Table 2 shows the compositions of the Tospearl and PMPS samples pyrolyzed in both pure Ar and Ar + H_2O atmospheres at 1400 °C. The Ar pyrolyzed Tospearl sample has 9.74 wt% free carbon, much lower than the Ar pyrolyzed PMPS sample, which has 45.8 wt% carbon. In addition, the Ar + H_2O pyrolysis leads to significantly lower free C amounts, 0.5 wt% for the Tospearl sample and 37.4 wt% for the PMPS sample. Both results are expected as PMPS is a very C-rich precursor and the Ar + H_2O pyrolysis removes C-containing radicals at low temperatures.

Based on the Gibbs free energy minimization method presented in this study, contents of free carbon and other phases (from SiC-SiO_2 tie-line) for various SiOC compositions can be calculated using Eq. (14) and the Gibbs free energy minimization method respectively. It shows that the Ar pyrolyzed Tospearl sample has 52.6% SiO_2, 28.7% $SiO_{3/2}C_{1/4}$, 7.5% $SiOC_{1/2}$, and 0% $SiO_{1/2}O_{3/4}$. For the Ar pyrolyzed PMPS sample, the SiO_2 content is only 7.7%, the $SiO_{3/2}C_{1/4}$ phase content is only 12.9% while the $SiOC_{1/2}$ and $SiO_{1/2}C_{3/4}$ contents increase to 13.1% and 13.4%, respectively. Interestingly, both samples have very similar SiC

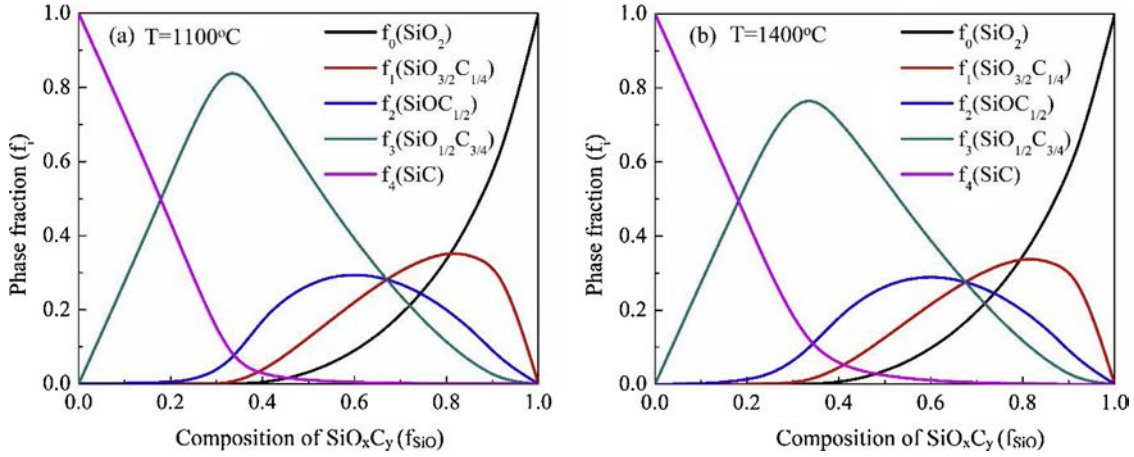

Fig. 7. Fraction of different amorphous SiOC compounds, amorphous SiO_2, and crystalline SiC vs. the composition of SiO_xC_y: (a) 1100 °C, (b) 1400 °C.

Table 2
SiOC compositions and corresponding phase contents after pyrolysis at 1400 °C.

Sample	Composition (wt%)			Phase percent (%)					% Free carbon
	Si	O	C	SiO_2	$SiO_{\frac{3}{2}}C_{\frac{1}{4}}$	$SiOC_{\frac{1}{2}}$	$SiO_{\frac{1}{2}}C_{\frac{3}{4}}$	SiC	
PMPS (Ar-1400 °C)	32.6	21.6	45.8	7.7	12.9	13.1	13.4	0.4	52.6
PMPS (Ar + H_2O-1400 °C)	31.7	30.9	37.4	30.4	15.9	4.5	1.2	0.2	47.7
TP (Ar-1400 °C)	45.8	44.5	9.7	52.6	28.7	7.5	0.0	0.4	10.8
TP (Ar + H_2O-1400 °C)	45.9	53.6	0.5	99.2	0.0	0.0	0.0	0.0	0.8

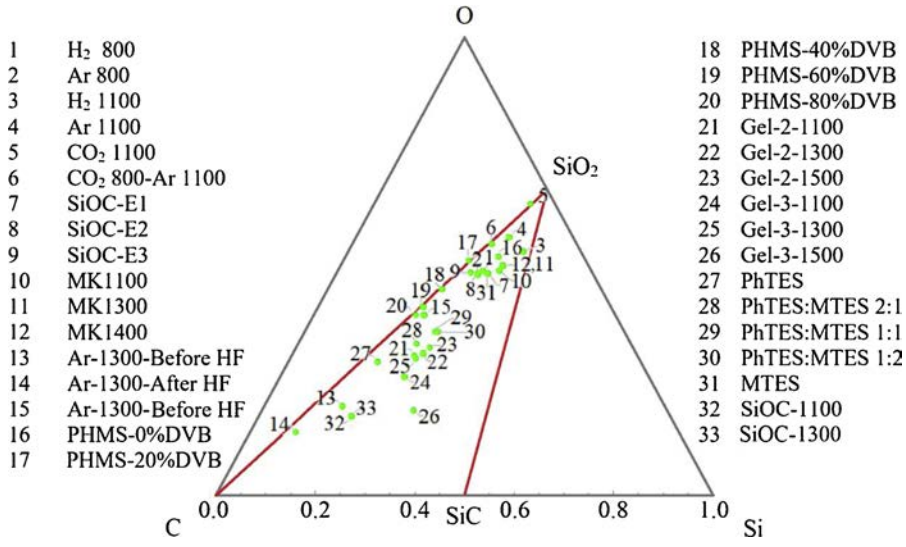

Fig. 8. Ternary composition diagram showing various SiOC systems from the literature. The specific references are given in Table 3 for each sample.

content. A high free C content leads to higher contents of $SiOC_{1/2}$ and $SiO_{1/2}C_{3/4}$ phases while a high SiO_2 content also means a higher amount of the $SiO_{3/2}C_{1/4}$ phase. For the Tospearl and PMPS samples pyrolyzed in Ar + H_2O, the free C content decreases significantly. For the Tospearl sample, the free carbon amount is only 0.8%. The pyrolysis of PMPS with Ar + H_2O atmosphere shows reduced free carbon from 52.6% to 47.7%. However, the amount is still much higher compared to the Tospearl samples. At the same time, the SiO_2 phase for the PMPS sample increases to 30.4% while for the Tospearl sample it increases to 99.2%. This means that most of the Tospearl has been converted to SiO_2 along with the formation of a small amount of free carbon. Since the sample is predominantly SiO_2, at the high temperature of 1400 °C, it crystallizes into cristobalite even with a low driving energy for crystallization. The PMPS sample shows significant increase in the SiO_2 phase in the Ar + H_2O atmosphere (30.4%) as compared to that of argon (7.7%). Both samples show significant amounts of intermediate amorphous SiOC compounds. The TEM images in Fig. 3 show SiC crystallites in the microstructure. The estimated SiC phase percent for the PMPS sample is 0.2% for the Ar + H_2O atmosphere.

To show the broad applicability of the phase content prediction method for the SiOC system, Fig. 8 shows locations of various SiOC compositions obtained from literature in the ternary composition diagram. As expected, all the compositions fall within the C-SiO_2-SiC composition triangle. Table 3 shows the phase fractions of these SiOC compositions calculated using the current approach. It shows that the phase fractions are affected by the polymer precursor, the pyrolysis temperature, and the pyrolysis atmosphere. In general, the SiC phase content is very low. The only exception is $SiO_{0.61}C_{1.67}$ (#26). Due to its low oxygen content, the SiC phase percent is highest, at 4.8%. In general, a higher SiO_2 content also means more $SiO_{3/2}C_{1/4}$. A higher SiC content also means higher $SiOC_{1/2}$ and $SiO_{1/2}C_{3/4}$ contents. A H_2 atmosphere (#3) also encourages equal phase amounts for $SiO_{3/2}C_{1/4}$, $SiOC_{1/2}$, and $SiO_{1/2}C_{3/4}$. CO_2 atmosphere pyrolysis can only lead to the formation of free carbon and SiO_2 (#5 and #6). Simply increasing the pyrolysis temperature (#23) is not conducive for SiC formation. Reducing O content in a given SiOC system is key for SiC formation (#26, #33).

4. Conclusions

The effects of pyrolysis atmosphere on the phase formation of SiOC from different precursors are investigated at pyrolysis temperatures up to 1400 °C. For the high C-containing polymer precursors, PMPS and PVMS, the water vapor treatment has little influence on the phase formation between 1100 °C–1400 °C compared to Ar, with the samples showing similar contents of SiO_2, SiC, and carbon. For the samples with intermediate carbon contents, PDMS and PHMS, the phase separation of the SiOC matrix into SiO_2, SiC, and carbon occurs at 1300 °C for the water vapor condition. In all cases, SiC formation is reduced in the water vapor pyrolysis condition. The only exception is the Tospearl sample, which crystallizes at 1400 °C into cristobalite for the water vapor condition. From a thermodynamic viewpoint, phase evolution in both Ar and Ar + H_2O atmospheres can be understood based on the driving force for crystallization. Different phase contents at various pyrolysis conditions can be calculated based on a Gibbs free energy minimization method. The driving force for crystallization is highest for the Tospearl sample pyrolyzed in Ar + H_2O, which matches with the experimental findings.

Table 3
SiOC compositions and fractions of free carbon (f_c) and other phases (f_i) calculated using Eq. (14).

	Composition	Pyrolysis temperature and atmosphere	Phase percent (%)					% Free carbon	References
			SiO_2	$SiO_{\frac{3}{2}}C_{\frac{1}{4}}$	$SiOC_{\frac{1}{2}}$	$SiO_{\frac{1}{2}}C_{\frac{3}{4}}$	SiC		
1	$SiO_{1.67}C_{0.48}$	H_2, 800 °C	45.5	31.3	9.9	3.2	0.0	10.1	[32]
2	$SiO_{1.71}C_{0.65}$	Ar, 800 °C	48.0	27.9	7.2	1.9	0.0	15.1	
3	$SiO_{1.51}C_{0.25}$	H_2, 1100 °C	36.9	35.9	17.9	9.1	0.1	0.2	
4	$SiO_{1.83}C_{0.38}$	Ar, 1100 °C	66.0	19.8	4.3	0.7	0.1	9.1	
5	$SiO_{2.02}C_{0.19}$	CO_2, 1100 °C	94.2	0.0	0.0	0.0	0.0	5.8	
6	$SiO_{1.96}C_{0.54}$	CO_2 up to 800 °C, then Ar till 1100 °C	81.2	2.8	0.8	0.3	0.1	14.8	
7	$SiO_{1.60}C_{0.70}$	N_2, 1000 °C	39.1	29.5	11.8	4.5	0.0	15.2	[33]
8	$SiO_{1.68}C_{0.80}$	N_2, 1000 °C	44.2	26.7	8.1	2.4	0.0	18.6	
9	$SiO_{1.81}C$	N_2, 1000 °C	52.7	20.1	4.5	0.8	0.0	21.9	
10	$SiO_{1.52}C_{0.57}$	Ar, 1100 °C	33.0	32.2	16.0	8.1	0.1	10.7	[34]
11	$SiO_{1.53}C_{0.53}$	Ar, 1300 °C	35.9	30.8	15.4	7.9	0.4	9.6	
12	$SiO_{1.53}C_{0.52}$	Ar, 1500 °C	37.2	30.1	15.3	7.8	0.2	9.4	
13	$SiO_{1.23}C_{4.15}$	Ar, 1300 °C, before HF etching	8.3	12.5	10.6	9.4	0.3	59.0	[15]
14	$SiO_{1.50}C_{8.41}$	Ar, 1300 °C, after HF etching	9.8	8.4	4.6	2.3	0.1	74.8	
15	$SiO_{1.77}C_{1.74}$	Ar + H_2O, 1300 °C, before HF etching	41.7	16.6	4.2	1.3	0.2	36.0	
16	$SiO_{1.68}C_{0.55}$	Ar, 1200 °C	48.0	27.3	9.3	3.3	0.1	12.1	[35]
17	$SiO_{2.02}C_{0.92}$	Ar, 1200 °C	76.6	0.0	0.0	0.0	0.0	23.4	
18	$SiO_{1.96}C_{1.39}$	Ar, 1200 °C	64.6	2.9	0.8	0.1	0.1	31.6	
19	$SiO_{1.94}C_{1.78}$	Ar, 1200 °C	56.6	4.4	1.2	0.4	0.2	37.1	
20	$SiO_{1.92}C_{1.95}$	Ar, 1200 °C	52.2	6.3	1.6	0.4	0.2	39.3	
21	$SiO_{1.25}C_{1.83}$	Ar, 1000 °C	12.7	20.4	17.0	14.2	0.0	35.7	[36]
22	$SiO_{1.18}C_{1.63}$	Ar, 1300 °C	11.4	19.4	18.7	18.1	0.5	31.9	
23	$SiO_{1.20}C_{1.52}$	Ar, 1500 °C	13.4	19.7	18.4	17.8	0.6	30.1	
24	$SiO_{1.03}C_{1.96}$	Ar, 1000 °C	6.6	15.3	18.4	22.6	0.1	37.1	
25	$SiO_{1.17}C_{1.77}$	Ar, 1300 °C	11.0	18.7	18.0	17.4	0.5	34.3	
26	$SiO_{0.61}C_{1.67}$	Ar, 1000 °C	0.7	3.2	12.2	48.8	5.4	29.7	
27	$SiO_{1.63}C_{2.95}$	Ar, 1000 °C	24.3	17.7	6.2	2.2	0.0	49.6	[37]
28	$SiO_{1.39}C_{1.82}$	Ar, 1000 °C	17.8	22.2	14.9	9.2	0.0	35.9	
29	$SiO_{1.36}C_{1.45}$	Ar, 1000 °C	18.6	24.3	16.4	11.0	0.0	29.6	
30	$SiO_{1.33}C_{1.40}$	Ar, 1000 °C	17.8	24.3	17.4	12.1	0.0	28.5	
31	$SiO_{1.58}C_{0.68}$	Ar, 1000 °C	37.5	30.1	12.7	5.2	0.0	14.5	
32	$SiO_{0.92}C_{3.45}$	Ar, 1100 °C	2.8	8.5	13.2	21.1	0.2	54.2	[38]
33	$SiO_{0.93}C_{3.45}$	Ar, 1300 °C	3.2	8.4	13.3	20.2	0.7	54.2	

Declarations of interest

None.

Acknowledgment

We acknowledge the financial support from National Science Foundation under grant number CMMI-1634325.

Appendix A. Supplementary data

Supplementary material related to this article can be found, in the online version, at doi:https://doi.org/10.1016/j.jeurceramsoc.2019.03.032.

References

[1] J.K. Li, K. Lu, Highly porous SiOC bulk ceramics with water vapor assisted pyrolysis, J. Am. Ceram. Soc. 98 (8) (2015) 2357–2365.
[2] G.D. Soraru, R. Pena-Alonso, M. Leoni, C-rich micro/mesoporous Si(B)OC: in situ diffraction analysis of the HF etching process, Microporous Mesoporous Mater. 172 (2013) 125–130.
[3] M.A. Mazo, A. Tamayo, A.C. Caballero, J. Rubio, Electrical and thermal response of silicon oxycarbide materials obtained by spark plasma sintering, J. Eur. Ceram. Soc. 37 (5) (2017) 2011–2020.
[4] K. Lu, D. Erb, M. Liu, Thermal stability and electrical conductivity of carbon-enriched silicon oxycarbide, J. Mater. Chem. C 4 (9) (2016) 1829–1837.
[5] K. Lu, D. Erb, M.Y. Liu, Phase transformation, oxidation stability, and electrical conductivity of TiO_2-polysiloxane derived ceramics, J. Mater. Sci. 51 (22) (2016) 10166–10177.
[6] J. Cordelair, P. Greil, Electrical conductivity measurements as a microprobe for structure transitions in polysiloxane derived Si−O−C ceramics, J. Eur. Ceram. Soc. 20 (12) (2000) 1947–1957.
[7] A. Vomiero, S. Modena, G.D. Soraru, R. Raj, Y. Blum, G. Della Mea, Investigation on the oxidation process of SiCO glasses by the means of non-Rutherford backscattering spectrometry, Nucl. Instrum. Methods B 211 (3) (2003) 401–407.
[8] P.H. Mutin, Control of the composition and structure of silicon oxycarbide and oxynitride glasses derived from polysiloxane precursors, J. Sol-Gel Sci. Technol. 14 (1) (1999) 27–38.
[9] R. Campostrini, G. DAndrea, G. Carturan, R. Ceccato, G.D. Soraru, Pyrolysis study of methyl-substituted Si−H containing gels as precursors for oxycarbide glasses, by combined thermogravimetry, gas chromatographic and mass spectrometric analysis, J. Mater. Chem. 6 (4) (1996) 585–594.
[10] M. Narisawa, T. Kawai, S. Watase, K. Matsukawa, T. Dohmaru, K. Okamura, A. Iwase, Long-lived photoluminescence in amorphous Si−O−C(−H) ceramics derived from polysiloxanes, J. Am. Ceram. Soc. 95 (12) (2012) 3935–3940.
[11] Y. Blum, G.D. Soraru, A.P. Ramaswamy, D. Hui, S.M. Carturan, Controlled mesoporosity in SiOC via chemically bonded polymeric "spacers", J. Am. Ceram. Soc. 96 (9) (2013) 2785–2792.
[12] D. Hourlier, S. Venkatachalam, M.R. Ammar, Y. Blum, Pyrolytic conversion of organopolysiloxanes, J. Anal. Appl. Pyrol. 123 (2017) 296–306.
[13] W.R. Schmidt, L.V. Interrante, R.H. Doremus, T.K. Trout, P.S. Marchetti, G.E. Maciel, Pyrolysis chemistry of an organometallic precursor to silicon-carbide, Chem. Mater. 3 (2) (1991) 257–267.
[14] T.A. Liang, Y.L. Li, D. Su, H.B. Du, Silicon oxycarbide ceramics with reduced carbon by pyrolysis of polysiloxanes in water vapor, J. Eur. Ceram. Soc. 30 (12) (2010) 2677–2682.
[15] K. Lu, J.K. Li, Fundamental understanding of water vapor effect on SiOC evolution during pyrolysis, J. Eur. Ceram. Soc. 36 (3) (2016) 411–422.
[16] D. Erb, K. Lu, Additive and pyrolysis atmosphere effects on polysiloxane-derived porous SiOC ceramics, J. Eur. Ceram. Soc. 37 (15) (2017) 4547–4557.
[17] M. Narisawa, F. Funabiki, A. Iwase, F. Wakai, H. Hosono, Effects of atmospheric composition on the molecular structure of synthesized silicon oxycarbides, J. Am. Ceram. Soc. 98 (10) (2015) 3373–3380.
[18] S. Martinez-Crespiera, E. Ionescu, H.J. Kleebe, R. Riedel, Pressureless synthesis of fully dense and crack-free SiOC bulk ceramics via photo-crosslinking and pyrolysis of a polysiloxane, J. Eur. Ceram. Soc. 31 (5) (2011) 913–919.
[19] K. Lu, Porous and high surface area silicon oxycarbide-based materials—a review, Mater. Sci. Eng. R 97 (2015) 23–49.
[20] X.Y. Yuan, H.L. Jin, X.B. Yan, L.F. Cheng, L.T. Hu, Q.J. Xue, Synthesis of ordered mesoporous silicon oxycarbide monoliths via preceramic polymer nanocasting, Microporous Mesoporous Mater. 147 (1) (2012) 252–258.
[21] H.J. Kleebe, C. Turquat, G.D. Soraru, Phase separation in an SiCO class studied by

transmission electron microscopy and electron energy-loss spectroscopy, J. Am. Ceram. Soc. 84 (5) (2001) 1073–1080.
[22] E. Ionescu, B. Papendorf, H.J. Kleebe, F. Poli, K. Muller, R. Riedel, Polymer-derived silicon oxycarbide/hafnia ceramic nanocomposites. Part I: phase and microstructure evolution during the ceramization process, J. Am. Ceram. Soc. 93 (6) (2010) 1774–1782.
[23] Y.D. Blum, D.B. MacQueen, H.J. Kleebe, Synthesis and characterization of carbon-enriched silicon oxycarbides, J. Eur. Ceram. Soc. 25 (2–3) (2005) 143–149.
[24] R. Pena-Alonso, G.D. Soraru, R. Raj, Preparation of ultrathin-walled carbon-based nanoporous structures by etching pseudo-amorphous silicon oxycarbide ceramics, J. Am. Ceram. Soc. 89 (8) (2006) 2473–2480.
[25] Y.D. Blum, D.B. MacQueen, H.-J. Kleebe, Synthesis and characterization of carbon-enriched silicon oxycarbides, J. Eur. Ceram. Soc. 25 (2–3) (2005) 143–149.
[26] G. Gregori, H.J. Kleebe, Y.D. Blum, F. Babonneau, Evolution of C-rich SiOC ceramics—part II. Characterization by high lateral resolution techniques: electron energy-loss spectroscopy, high-resolution TEM and energy-filtered TEM, Int. J. Mater. Res. 97 (6) (2006) 710–720.
[27] J.A. Golczewski, F. Aldinger, Thermodynamic modeling of amorphous Si—C—N ceramics derived from polymer precursors, J. Non-Cryst. Solids 347 (1-3) (2004) 204–210.
[28] M.W. Chase Jr., NIST-JANAF Thermochemical Tables, fourth edition, American Chemical Society, American Institute of Physics for the National Institute of Standards and Technology, Washington, DC, New York, 1998.
[29] G. Foti, Silicon carbide: from amorphous to crystalline material, Appl. Surf. Sci. 184 (1) (2001) 20–26.
[30] K. Tapasa, T. Jitwatcharakomol, Thermodynamic calculation of exploited heat used in glass melting furnace, Procedia Eng. 32 (2012) 969–975.
[31] A.H. Tavakoli, M.M. Armentrout, M. Narisawa, S. Sen, A. Navrotsky, White Si—O—C ceramic: structure and thermodynamic stability, J. Am. Ceram. Soc. 98 (1) (2015) 242–246.
[32] M. Narisawa, F. Funabiki, A. Iwase, F. Wakai, H. Hosono, T. Besmann, Effects of atmospheric composition on the molecular structure of synthesized silicon oxycarbides, J. Am. Ceram. Soc. 98 (10) (2015) 3373–3380.
[33] K. Yamamoto, J. Ohshita, T. Mizumo, T. Tsuru, Efficient synthesis of SiOC glasses from ethane, ethylene, and acetylene-bridged polysilsesquioxanes, J. Non-Cryst. Solids 408 (2015) 137–141.
[34] R. Riedel, L. Toma, E. Janssen, J. Nuffer, T. Melz, H. Hanselka, Piezoresistive effect in SiOC ceramics for integrated pressure sensors, J. Am. Ceram. Soc. 93 (4) (2010) 920–924.
[35] K. Lu, D. Erb, M.Y. Liu, Thermal stability and electrical conductivity of carbon-enriched silicon oxycarbide, J. Mater. Chem. C 4 (9) (2016) 1829–1837.
[36] K.D. Xia, C.X. Lu, Y. Yang, B.P. Zhang, Effect of vinyltriethoxysilane addition on the pyrolytic conversion of tetraethoxysilane based silica gel, J. Sol-Gel Sci. Technol. 69 (2) (2014) 266–271.
[37] M. Wilamowska, V.S. Pradeep, M. Graczyk-Zajac, R. Riedel, G.D. Sorarù, Tailoring of SiOC composition as a way to better performing anodes for Li-ion batteries, Solid State Ionics 260 (2014) 94–100.
[38] J. Kaspar, M. Graczyk-Zajac, R. Riedel, Carbon-rich SiOC anodes for lithium-ion batteries: part II. Role of thermal cross-linking, Solid State Ionics 225 (2012) 527–531.